View metadata, citation and similar papers at core.ac.uk
brought to you by CORE
provided by CiteSeerX

Proceedings of GT2007
ASME Turbo Expo 2007: Power for Land, Sea and Air
May 14-17, 2007, Montreal, Canada

GT2007-27148

IMPACT OF RADIATION ON THE WALL HEAT LOAD AT A TEST BENCH GAS TURBINE COMBUSTION CHAMBER: MEASUREMENTS AND CFD SIMULATION

R. Dannecker
DLR German Aerospace Center,
Institute of Combustion Technology, Stuttgart

B. Noll
DLR German Aerospace Center,
Institute of Combustion Technology, Stuttgart
Corresponding author: Berthold.Noll@dlr.de

M. Hase, W. Krebs
Siemens AG Power Generation,
Mülheim/Ruhr

K.-U Schildmacher
Siemens AG Power Generation,
Mülheim/Ruhr

R. Koch
University of Karlsruhe,
Institute of Thermal Turbomachinery

M. Aigner
DLR German Aerospace Center,
Institute of Combustion Technology, Stuttgart

ABSTRACT

Experimental and numerical work has been carried out to determine the wall heat load at the liner structure of a model gas turbine combustion chamber. Measured cross-sectional profiles of the velocity and temperature field inside the chamber could be used to validate various CFD calculations of the combustion flow. It turned out that only a special treatment of the thermal boundary conditions at all liner walls would actually lead to appropriate values of the wall heat flux. Radiation modeling included two radiative properties models (SG single gray gas and WSSG weighted sum of gray gases) and three radiation transport models (P1, DT discrete transfer, MC Monte Carlo). The performance of the WSGG model has been assessed with charts and the impact of the radiation on the liner wall temperature distribution has been studied. The experimental values are matched within 3% deviation with the best combination of transport and radiation property models. The radiation contributes to 20-30% of the total wall heat flux. The present approach enables Siemens PG to access the thermal design of combustors more precisely.

Keywords combustor simulation, wall heat load, heat radiation

NOMENCLATURE

L	characteristic length
P	operation pressure
p	partial pressure
p_{CO2}	partial pressure of CO_2
p_{H2O}	partial pressure of H_2O
q	heat flux
SG	single gray
T	temperature
$T_{av.wall}$	area mean wall temperature
T_{blade}	exhaust channel wall temperature
TRI	turbulence-radiation interaction
X	molar concentration
x	axial coordinate
z	coordinate
V	velocity
WSGG	Weighted sum of gray gases
ε	emissivity coefficient
κ	absorptivity coefficient
ϕ	equivalence ratio
Φ	cooling effectiveness

INTRODUCTION

With regard to the rising world wide energy demand coupled with climbing fuel expenses and urgent environmental aspects the development of high efficient environmentally compatible gas turbines has high priority for the power plant industry all over the world. The so-called lean premixed combustion technique offers high potential to realize high efficiency at high temperatures and pressures together with low

Copyright © 2007 by ASME

Downloaded From: https://proceedings.asmedigitalcollection.asme.org on 07/01/2019 Terms of Use: http://www.asme.org/about-asme/terms-of-use

NO_x emission. Due to high air consumption in the combustion process at lean mixtures high high priority is given to optimize the cooling air management. Thus a reliable prediction of wall heat load becomes crucial in the design process of such a combustor. Besides convective heat transfer the combustor liner can also suffer considerably from radiative heat load.

An accurate simulation of radiative processes requires the knowledge of the temperature and species distributions which can be obtained by multidimensional combustion CFD methods. The quality of predicted radiative processes thus depends on the quality of the numerically calculated temperature and species fields. However, it also depends on the quality of the employed models for radiative transfer and radiative properties.

Despite the fact that radiation can be very important for the design of combustion chambers there is only very little experimental and simulation data available in the open literature concerning the effect of heat radiation on the thermal loading of the wall liners and the gas temperature field of gas turbine combustion chambers [1-3]. Thus, it can be concluded that there is not much known about the effects of radiation and the accuracy of the available numerical tools for radiative processes within modern gas turbine chambers.

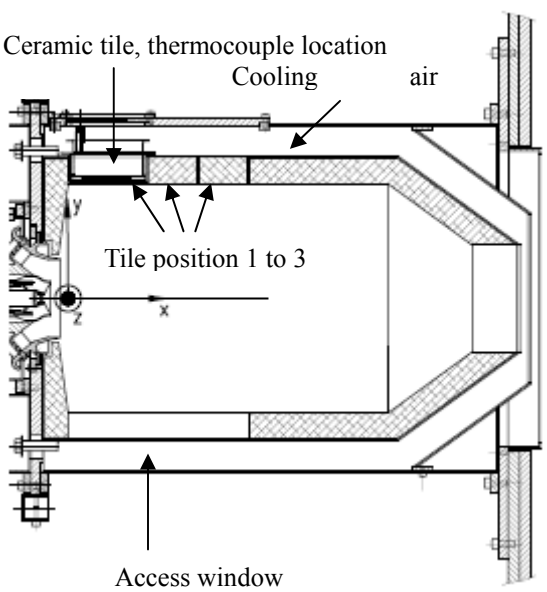

Figure 1: Scetch of combustion chamber and co-ordinate system

The present paper addresses the role of radiative heat load of gas turbine combustors walls. In particular, the accuracy of different radiation models is evaluated. In a research program an experimental and numerical investigation has been carried out on an atmospheric test rig with one single Siemens burner.

EXPERIMENTAL SET-UP

The single burner was mounted to the atmospheric test rig at the ITS, University of Karlsruhe [4], and 19 thermocouples (type S, PtRh10-Pt) were placed within a ceramic liner tile in order to measure the heat flux through the 40 mm thick ceramic tile. Here, 8 thermocouples were placed at the inner face, 8 at the outer face and three in the middle of the ceramic. The thermoelectric voltage was converted into temperature according DIN EN 60581-1. In the course of the experiment, the ceramic tile with the thermocouples mounted was displaced in axial direction along the liner wall in order to take measurements at three different positions (figures 1 and 2). Hence, the measurements on the wall covered nearly half of the axial chamber span. The outer face of the ceramic tile and the combustion chamber are surrounded by a cooling air flow. The major objective of this air flow is to reduce the exhaust gas temperature in order to prevent overheating of the chimney. On the other side it ensures a well defined thermal boundary condition of the ceramic tile. However, compared to the thermal load of the combustor the heat flux through the tile is very small.

The chamber was accessible in order to take measurements of the cross-sectional profiles of the temperature and velocity fields inside the chamber (fig. 1). Velocity measurements were taken with LDA [4, 5], temperature was measured with a probe. Corrections for radiation effects were introduced in the temperature measurements.

EXPERIMENTAL BOUNDARY CONDITIONS

The chamber was operated with natural gas. In pre-mixed operation condition, the flame was stabilized by 7 % pilot gas injection, 93% of the gas was injected through the premixing gas nozzle. The air was preheated to 673 K which corresponds to a typical burner inlet temperature of gas turbines. The air volume flow was set to that of a burner in the engine under typical pressurized conditions in order to ensure Mach number similarity. The Re-number at the burner nozzle was in the range of 10^5. More details about the rig and the burner design are described in [4, 5].

Total thermal power	450 kW
Operation pressure	1 bar
Equivalence ratio ϕ	0.5
Cooling air inlet conditions	337 K, 13.7 m/s
Ratio cooling air / combustion air	4:1

The thermal conductivity of the ceramic tile was given by the manufacturer as a function of temperature (fig. 2).

With increasing temperature the thermal conductivity of ceramics decreases, which is a typical characteristic for electrical isolators [6] and differs here from the characteristic of steel or gases. During lean combustion the ceramics remains reflective with an emissivity of 0.4. The major heat flux of the tile is in the perpendicular direction, which is at least ten times

Copyright © 2007 by ASME

Downloaded From: https://proceedings.asmedigitalcollection.asme.org on 07/01/2019 Terms of Use: http://www.asme.org/about-asme/terms-of-use

higher than that in lateral direction. The mean cooling effectiveness of the tile cooling system, which is defined as $\Phi=(T_{gas}-T_{outer\ wall})/(T_{gas}-T_{coolant})$, is in range of 0.68.

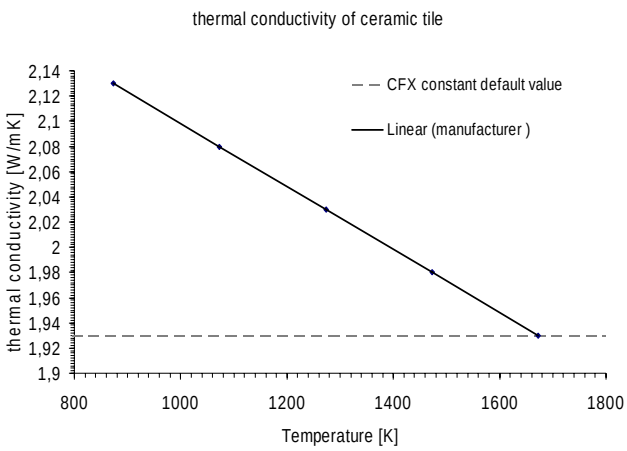

Figure 2: thermal conductivity of ceramics

CFD SET-UP AND BOUNDARY CONDITIONS

All CFD calculations were carried out with the commercial software package Ansys-CFX, the grid was generated with the CFX related software ICEM.

Turbulence was modeled with the standard k-ε model, which turned out to compare favorable with experimental results. Combustion was modeled with the eddy dissipation model.

GRID

The combustion chamber including the burner nozzle was modeled with a 3D grid consisting of about 720000 cells. The double swirler of the burner with its blades was not explicitly modeled, instead a boundary inflow profile provided by Siemens was deployed. As can be seen in fig.3, the upper liner wall where the thermocouples where placed has been included into the computational domain. The grid of the flow domain is not symmetrical; it is refined in the upper half of the domain and in particular towards the upper ceramic boundary, where in the experiment the thermocouples were located. In a preliminary investigation, the convective heat transfer on a uniform and symmetrical grid with about 1780000 cells has been compared with the results calculated on the grid of 720000 in fig.3, and there was no significant deviation of the wall temperatures at the ceramic conjugate heat transfer boundary (the upper wall). This may be due to the fact, that the calculation was carried out with the k-ε model using the so called scaleable wall functions. With scalable wall function the grid sensitivity is significantly reduced [7].

INFLOW BOUNDARY

As stated above, an inflow profile was deployed according to the data provided by the manufacturer of the burner nozzle. The direction of the inflow through both inlets (axial and diagonal, compare fig.4) has been adapted to model a co-rotating double swirl as generated from the burner. The piloting gas fraction (7% of the total amount of CH_4) has been distributed in the model equally over the axial inlet, the diagonal premixing passage contained 93% of the total amount of methane. The overall equivalence ratio was $\phi = 0{,}50$. Preheating and operation pressure was set according to the experiment.

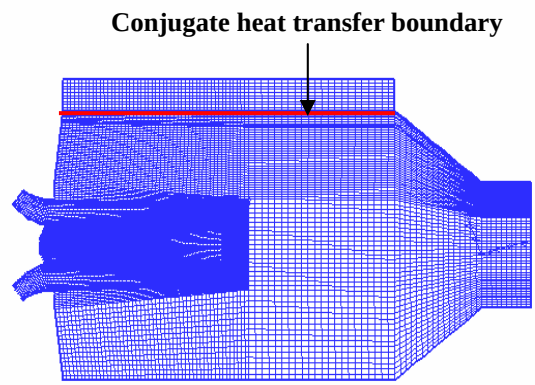

Figure 3: Non-uniform grid of the combustion chamber

For the turbulent inlet conditions, the fractional intensity was estimated as 0.05 and the eddy length scale was based on geometrical details of the burner.

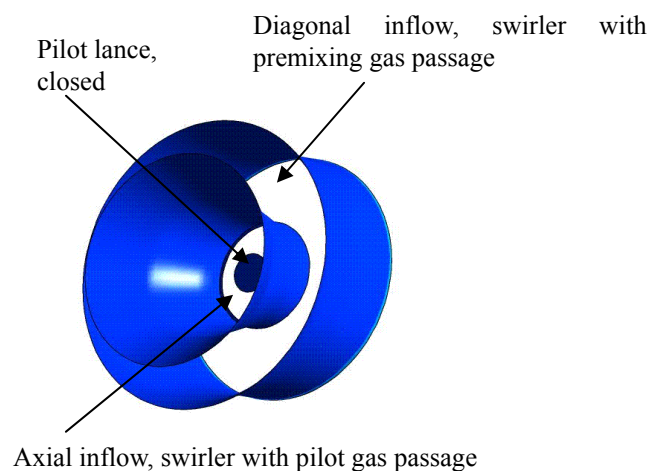

Figure 4: Burner nozzle, CFD model (cf. fig.1)

In the experiment, closed steel tubing and a closed steel plenum supplies the inflow. Hence, as boundary condition for

Copyright © 2007 by ASME

Downloaded From: https://proceedings.asmedigitalcollection.asme.org on 07/01/2019 Terms of Use: http://www.asme.org/about-asme/terms-of-use

radiation it was assumed that the ambient environment at the inflow functions as a black body radiator at inflow temperature.

WALL BOUNDARY

At all liner walls the boundary condition for the momentum equation was set to non-slip for a smooth wall. In order to insure equal energy transfer conditions at all liner walls, a special thermal boundary condition was applied at all liner walls, which were not subject to explicitly calculated conjugate heat transfer. The temperature of the cold gas side was interpolated (fig.5) based on the provided experimental values and applied to all liner walls. All other energy boundary options, like fixed T, adiabatic or fixed heat flux, caused unrealistic heat flux values across the liner. As soon as radiation is involved, the thermal equilibrium depends on equal treatment of all wall boundaries, and the conjugate heat transfer boundary at one wall needs to be complemented by at least 1D heat flux boundary condition at all walls.

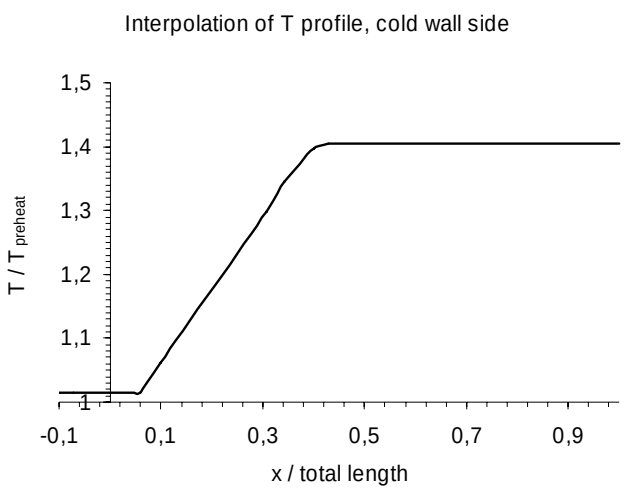

Figure 5: Temperature distribution on the cold gas side of the liner wall

The thermal conductivity of ceramics has been modeled either as function of the temperature or as constant value (fig. 2). In a preliminary investigation of the temperature dependence of the thermal conductivity of ceramics, the temperatures on the liner wall turned out to be around 20 K lower than the model with constant thermal conductivity.

The radiation boundary conditions for the opaque wall were estimated with an emissivity $\varepsilon = 0.4$ and a diffuse fraction of 1, since the ceramic tiles keep a pale surface with the lean combustion generating only very little amount of soot.

OUTLET BOUNDARY

For the momentum field a static pressure condition was applied at the outlet, whereas the impact of various radiation outlet conditions has been investigated. If the ambient environment at the outlet is assumed to be at outlet temperature, a large amount of radiation enters the outlet and increases the heat flux across the liner walls. Hence, at the outlet a black body radiator has been assumed at temperature T_{blade} which was estimated for the exhaust channel walls behind the combustor. In general, the results were not sensitive to the radiation outlet boundary condition, as long as a black body radiation at temperatures lower than the hot gas side liner wall was applied.

RADIATION MODELING

RADIATIVE PROPERTIES MODELS

Two different models SG and WSGG were applied for the calculation of the radiative properties of the combustion gases. The SG model takes the gas radiation as a black or gray body radiation without any bands. It implies that the combustion air has the same radiative properties than the combustion products. In CFX the single gray emissivity or absorptivity is set via the absoption coefficient κ, whereas the absorptivity $\alpha=1-e^{-\kappa L}$ and κL is called optical density. By default of CFX $\kappa=1/m$ is set. The value of κ is problem-dependent and thus should be derived from preliminary calculations. However, the SG model is not expensive and is frequently used in particular in connection with P1 radiation transport; here CFX recommends an optical density of at least 1.

WSGG calculates the local emissivity ε as a function of the species concentrations (H_2O,CO_2,CO, unburned hydrocarbons) and the temperatures.

$$\varepsilon_g\left(N, T(r), p(r)\cdot L(r)\right) = \sum_{i=1}^{N} a_i(T(r))\cdot\left(1-e^{-k_i\cdot(p(r)_{H2O}+p(r)_{CO2}+p(r)_{CO})\cdot L(r)-\kappa_i\cdot p(r)_{HC}\cdot L(r)}\right)$$

N is the number of virtual gases, the weight a_I is a function of the temperature.

Values are fitted with charts e.g. according to Hottel [8]. It may well be, that the local emissivity has a different value in scattering media and/or in a media confined within a reflecting enclosure. The radiation transport model has to take these effects into account.

The model takes the operation pressure into account via Daltons law: partial pressure of the species $p = X \cdot P$, where X is the molar concentration of the species and P the operation pressure. The charts, which were used to fit the model, own the parameter p L up to 250 atm m. Additional line broadening due to high pressure does not play a significant role in particular at high temperatures [9]. Edwards proposed a relation $pL' = pLP^m$ for pressure correction of the parameter partial pressure times optical path length (fig.6). The model can be applied in a temperature range of 1200K to 2400K.

Copyright © 2007 by ASME

Downloaded From: https://proceedings.asmedigitalcollection.asme.org on 07/01/2019 Terms of Use: http://www.asme.org/about-asme/terms-of-use

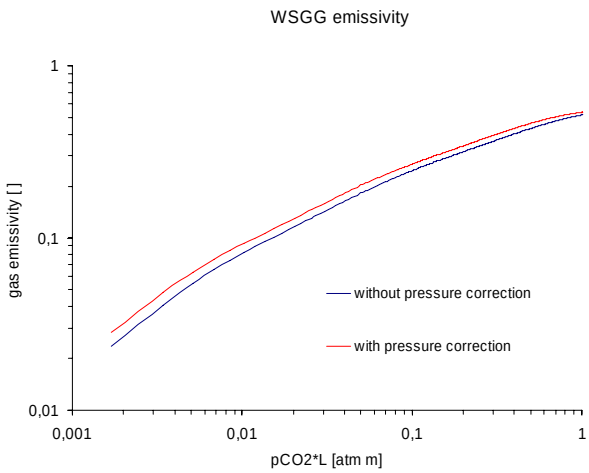

Figure 6: Edwards pressure correction with m=0.08

In fig.6 the change from experimental conditions at 1.7 atm to real scale conditions of 17 atm at a constant temperature of 1500K has been modeled for gas combustion, with the smallest optical path length of 0.001 m (compare pCO_2 L scale in fig. 6). The charts, which have been used to fit the model, display a total emissivity, there is no frequency resolution. However, the charts have been generated already for the mixture of CO_2 and H_2O, hence the line overlapp (e.g. at 2.7 µm) is already included in the fitting [8].

The pathlength L refers to a local value of a fluid control volume or a discretization length of the beam, which is larger than the cell size. Hence, the model determines emissivity as function of the local coordinate r, where r is in discrete values. Every radiation transport model „integrates“ over the beam path length. Hence, the equivalent optical density has to be calculated using a characteristic geometrical size of the chamber.

Several authors give different values for the coefficients and the weights. Mainly there are two sets of values, one for combustion of gas (partial pressure ratio of the products pH_2O/pCO_2 =2) (cf. fig.7) and one for oil and other fuel of the form $(CH_2)_x$ (with the partial pressure ratio of the products pH_2O/pCO_2 = 1).

Details to the model as used in CFX are given in the Manual of CFX [12] and refer to Taylor and Foster [10].

Non-gray models are dealt with treating each band as a separate calculation. The results of the bands are combined to give the total radiative heat transfer.

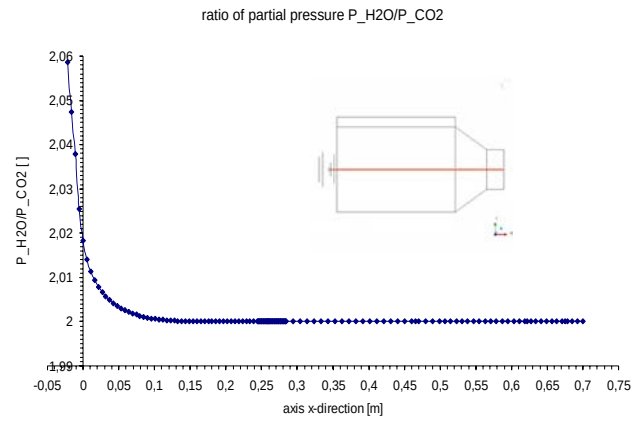

Figure 7: Partial pressure ratio of the products of simulated gas combustion, taken along the centeraxis of the chamber

RADIATION TRANSPORT MODELS

Three different radiation transport models have been applied: P1 model, the discrete transfer model and the Monte-Carlo method.

The P1 model is the first order approximation of the general PN-approximation using the method of spherical harmonics. Theoretical details are given in Modest [11]. Radiative transfer depends on the distribution of gas temperature and radiative properties and is governed by an integro-differential equation with several independent variables, which are the wave number, three space coordinates and two directional angular coordinates. The basic idea is that the solution of the radiative transfer equation can be simplified by expressing the radiative intensity in a series of products of angular (directional) and spatial coordinates. For the angular dependence spherical harmonical functions are used, which satisfy the Laplace equation in spherical coordinates. The spherical harmonical functions contain the polar and the azimuthal angles and the associated Legendre polynominals P_l^m. The number of terms l retained in the series expansion gives the method its name and its order [11]. In this way the method transforms the Radiation Transfer Equation into a set of simultaneous partial differential equations.

The method allows nonblack surfaces, nonconstant radiation properties, anisotropic scattering. However, the method requires near isotropic radiative intensity. The method may be in error in optically thin media with strongly anisotropic intensity distributions, in multidimensional geometries with large aspect ratio, and/or when surface emission dominates over the flow medium emission. However, when emission from a hot flow medium is considered, the P1 method leads to good results for optical thin medium but may even fail for optical thick medium. It gives good results for hot, radiating media in cold surroundings. The P1 approximation can lose accuracy when an optically thin medium acts as a

Copyright © 2007 by ASME

Downloaded From: https://proceedings.asmedigitalcollection.asme.org on 07/01/2019 Terms of Use: http://www.asme.org/about-asme/terms-of-use

radiation barrier between hot and cold surfaces. The P1 approximation does not work for collimated irradiation (= anisotropic). Improvements of the method exist but they are not implemented in CFX so far. The CFX recommendation is to use the P1 model only for an optical thickness > 1.

The Discrete Transfer Model of the radiation transfer in a three dimensional field with known temperature and known emissivity is based on discretization of the Radition Transfer Equation along rays. A description of the method is given by Modest [11] and by CFX [12]. The path along a ray is discretized by using the sections formed from breaking the path at fluid control volumes. It is important that the fluid control volumes are so small that the optical properties respectively the radiation field and the temperature inside the fluid control volume is homogenous and the scattering optical depth is less than 1 across the fluid control volume. The ray traversing the fluid control volume interacts with the volume depending on its pathlength through the volume: depositing energy into the volume weakens the ray, emission and in-scattering from the volume strengthens the ray. The fluid control volumes are clusters of grid cells, the method is computationally too expensive when too many volumes are crossed by rays. CFX applies here a method to coarsen the grid for radiation modeling, generating so called radiation elements, and the radiation field is calculated at a different (lower) frequency than the other transport equations. Coarsening factors can be set by the user.

Rays are traced from surface to surface. A boundary surface element consists of a cluster of boundary cell faces. The rays are leaving from nodal points at the boundary surface element. The unitary hemisphere over the boundary surface element is discretized using spherical coordinates. The span is divided into angles by the number of rays (in CFX by default 8), and ray directions are computed to pass through the center of the angles. The surface element (span x span) on the unitary hemisphere is then by default discretized by 8 x 8 rays. On the other side, the radiation intensity approaching a point on a boundary surface element is integrated over the hemispherical solid angle. The net radiative heat flux from the surface element is computed as $q_{out} = (1-\varepsilon_{wall})\, q_{in} + \varepsilon_{wall}\, \sigma\, T_{wall}^4$. The ray paths are calculated once and stored. The number of rays is to choose.

The model suits to nearly all optical properties and fails only at extremely optical thin (transparent) media. Optimized accuracy can be achieved with better radiation grid resolution (coarsening factor lower) and with a higher number of rays, which improves the shadow effect in complex geometries. Due to the discretization the method is susceptible to ray effects.

Radiation transfer with the Monte Carlo method in a three dimensional field with known temperature and known emissivity is also based on the discretization of the Radiation Transfer Equation along rays. The method is explained in Siegel [13] and by CFX [12]. The path along a ray is discretized by using the sections formed from breaking the path at fluid control volumes similar to the discrete transfer method. The photon traversing along the ray across the fluid control volume interacts with the volume depending on its path length through the volume: depositing energy into the volume weakens the ray (absorption), elastic scattering changes its direction, emission and in-scattering from the volume strengthens the photon. Each interaction of the photon is called an event, and each event is weighted. The photon is tracked through the system until its weight falls below a certain threshold at which point its energy is depleted. This process (photon generation, sum of events, depletion) is called 'the history' of that photon in that system. The photons are leaving either from photon source points at the boundary surfaces element of the radiating face ore they are emitted from points within the medium. The Monte Carlo method differs from the Discrete Transfer method in the way the photon sources are generated at the boundary surface element of the radiating surface or within the radiating medium. A statistical sample of representative energy (or photon) bundles is emitted with different points of emission, energy (wavelength) of emission and direction. However, the energy of the photon bundle depends on the local temperature. A generalized radiation exchange factor is computed by tracing the history of the energy bundles.

The Monte Carlo radiation transport model suits to nearly all optical properties. The ordinary Monte Carlo method becomes inefficient for open configurations and highly reflective surfaces, in optically very thick media or if an optical thin media is externally irradiated. However, this can be overcome with the energy portioning method [11].

Optimized accuracy can be achieved with better radiation grid resolution (coarsening factor lower) and higher number of histories. It can be used for very complex geometries.

However, the scatter of the heat flux results is inversely proportional to the number of bundles absorbed by a boundary surface or volume radiation element. The number of bundles is therefore proportional to the number of volume radiation elements. For a good spatial resolution with small volume radiation element size a very large number of bundles must be applied.

VALIDATION OF THE WSGG MODEL

The WSGG model as The WSGG model as implemented in CFX has been coded separately and compared with data from Ludwigs as quoted in Taylor and Foster [10]. Fig. 8 shows that there is generally a good agreement between experimental values and the slopes of the model, at least in the range from 1200K to 2400K. Further, the WSGG emissivities have been calculated on the base of a simulated flow field of the combustion chamber, with temperature distribution,

Copyright © 2007 by ASME

Downloaded From: https://proceedings.asmedigitalcollection.asme.org on 07/01/2019 Terms of Use: http://www.asme.org/about-asme/terms-of-use

operation pressure and the distribution of species concentrations. Here, the emissivity values have been related to a standard optical pathlength of 0.1 respectively 1 m. The temperature in the field was in the range of 1575K to 1725K, and the values of the simulation correlate well with the parameter slopes of the model (fig. 8).

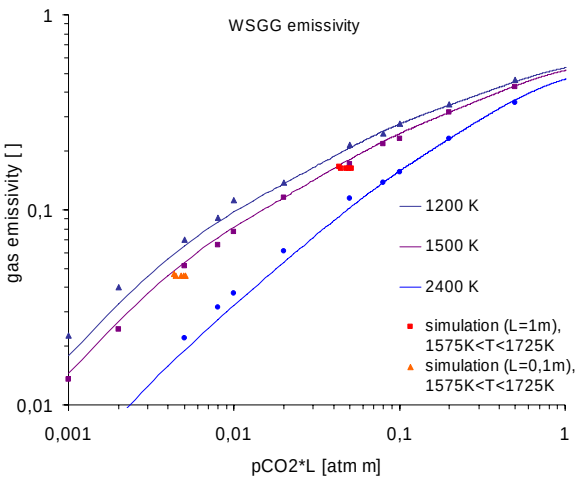

Figure 8: Validation of WSGG model and correlation with values of the simulated combustion chamber radiation field (lines: data from Ludwigs, s. [10])

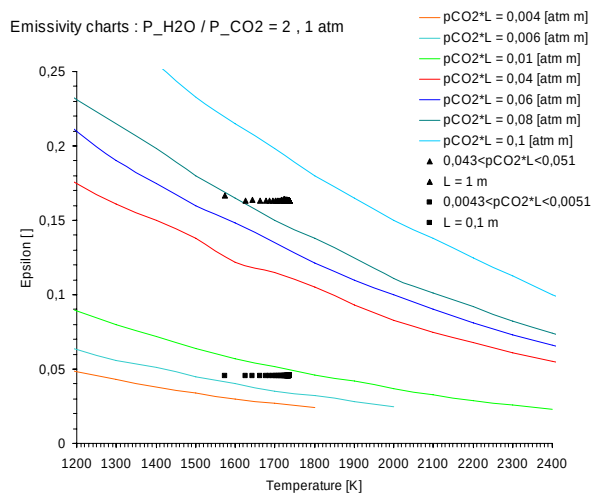

Figure 9: Correlation of simulated values to Hadvig charts [8]

The same values do not correlate so well with the charts of Hadvig [8], who generated the charts based on a mixture of H_2O and CO_2 from the original charts of Hottel after a unit conversion into SI units. The simulated emissivity values related to the standard optical pathlengths of 0.1m respectively 1m are overestimated, the values are expected to fit between the parameter slopes of $0.04 < p\,L < 0.06$, but they are above the slope $p\,L=0.06$ (fig. 9). However, for small optical pathlength the distance between the parameter slopes becomes very small and the absolute deviation of the simulated values from the chart values narrows down.

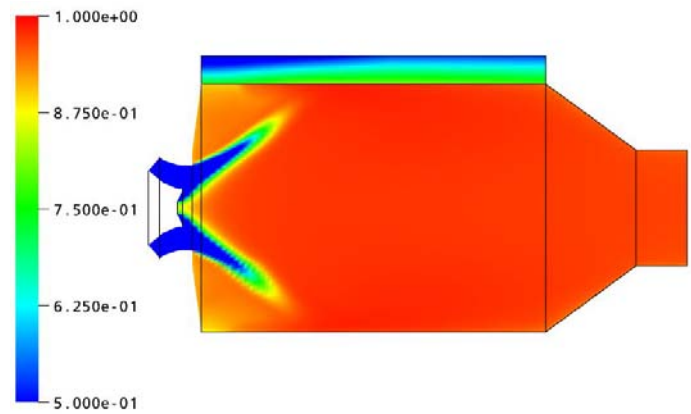

Figure 10: Simulated combustion with WSGG model and DT radiation transfer (T/T_max)

RADIATIVE AND CONVECTIVE WALL HEAT LOAD

In a first step, a pure convective solution, e.g. without considering radiation, was derived using the eddy dissipation combustion model. Here, the calculated temperature in the core of the flow field compared very well with the adiabatic flame temperature for the equivalence ratio of ϕ=0.50

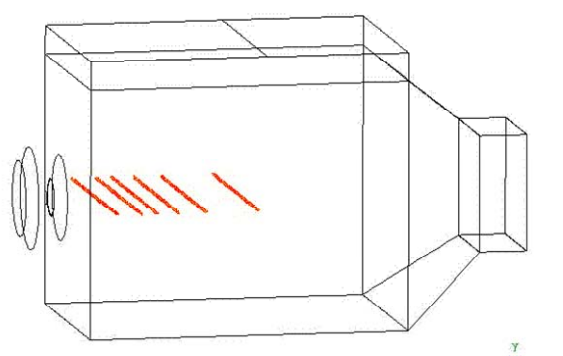

X1 = 0.06, X2 = 0.113, X3 = 0.147, X4 = 0.194,

Figure 11: Measurement positions in the chamber, x values refer to the total length

Based on the pure convective solution, further calculations comprising three different radiation transport models and two radiative properties models were carried out (e.g. fig. 10). The profiles of the velocity components and the temperature have been compared with experimental values at certain measurement positions (fig. 11). .

In the following section the profiles of temperature and of velocity components at the profile line X2 downstream of the burner nozzle will be shown. The profile is symmetrical to the central x-y plane, hence only half of the profile is displayed.

Copyright © 2007 by ASME

Downloaded From: https://proceedings.asmedigitalcollection.asme.org on 07/01/2019 Terms of Use: http://www.asme.org/about-asme/terms-of-use

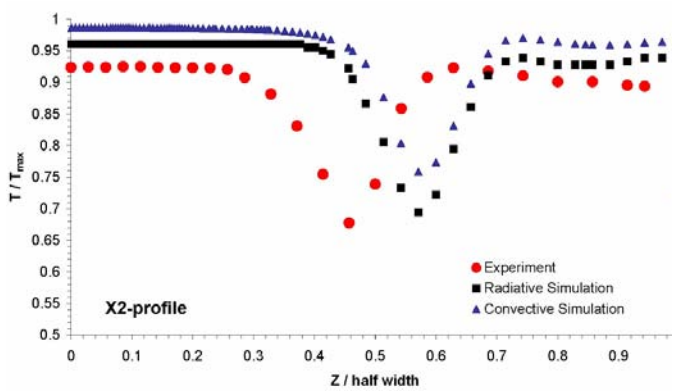

Figure 12: Temperature profile, T_{max} refers to the maximal temperature in the simulation

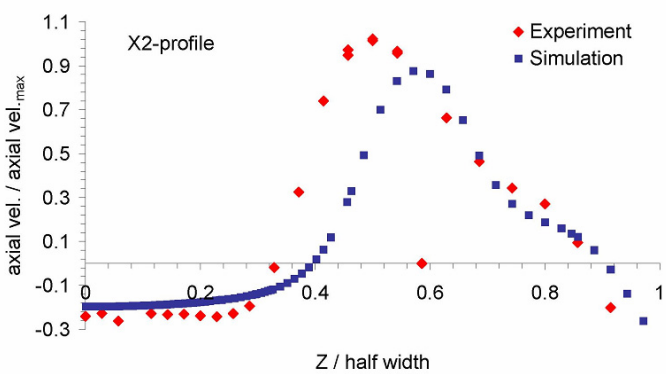

Figure 13: Axial velocity component, axial vel_{max} refers to the maximal axial velocity in the simulation

Fig.12 shows the comparison of the experimental data and the simulated values at measurement position X2 along one symmetrical half of the chamber line, z = 0 is on the chamber axis. The experimental and the simulated values appear to be misaligned in lateral direction, which appeared to be consistent throughout all measured data. The convective simulation meets the adiabatic flame temperature very well. The simulation including radiation predicts only slightly lower gas temperatures than the convective simulations. Thus, the calculation of radiation processes in a post processing step with a fixed velocity and species field is justified in the present case.

The calculation shown in fig. 12 is based on the WSGG model and it turned out a radiative source term of around 3% of the thermal power of 450 kW. The effect of radiation on the temperature of the ceramic liner wall is discussed further down.

Fig. 13 shows that except for a certain lateral shift between measurement and simulation satisfactory agreement of predicted and measured axial velocity components was achieved. In particular the recirculation zone in the core of the chamber and the outer recirculation zone are fairly well predicted.

The same applies to the tangential velocity component in fig. 14. The flow in the main stream with the maximal axial velocity component carries also the maximal tangential velocity, the recirculation zones carry only little swirl.

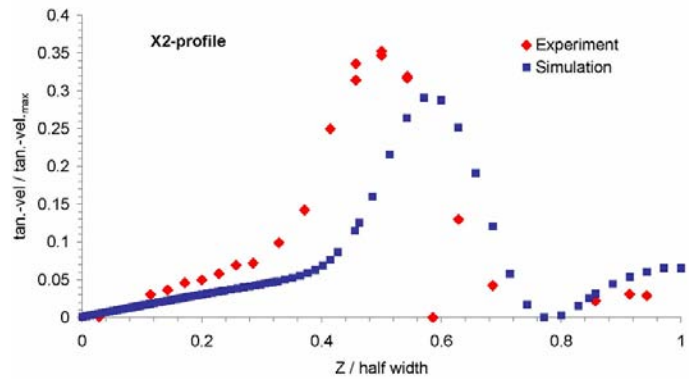

Figure 14: Tangential velocity component, $tan.\text{-}vel._{max}$ refers to the maxiamal tangential velocity in the simulation

The contour of the axial velocity component is shown in fig. 15. The non-uniform grid has only very little impact on the velocity field, in particular there is some small deviation at the outer recirculation zone.

Of particular interest was to determine the wall heat fluxes and the temperature at the interface to the ceramics for various combinations of the three radiation transport models with the two radiative properties models.

The experimental values of the temperature distribution at the ceramic interface (hot gas side) in fig. 16 are prone to an experimental uncertainty of about ±2% of the average wall temperature $T_{av,wall}$ as indicated in figs. 16-20.

A pure convective calculation fails to predict the correct wall temperature in particular at the front part of the wall (X/total length < 0.2).Here, the radiation changes the temperature distribution on the wall significantly.

The P1 radiation transport combined with single gray emissivity came closest to the experimental values; however it does not predict the shape of the distribution correctly. This model was used with the default absorption coefficient of 1/m,

Copyright © 2007 by ASME

Downloaded From: https://proceedings.asmedigitalcollection.asme.org on 07/01/2019 Terms of Use: http://www.asme.org/about-asme/terms-of-use

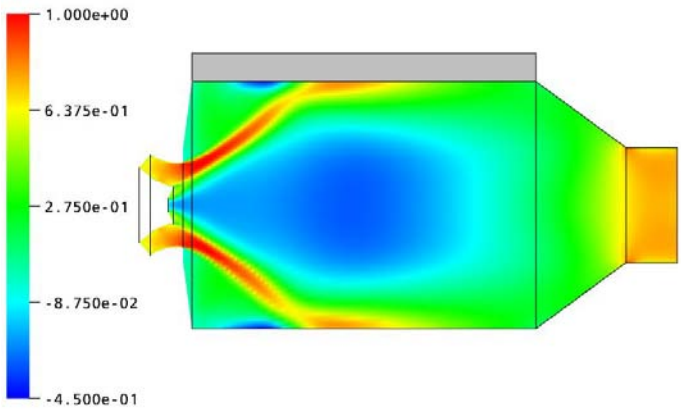

Figure 15: Axial velocity contour, simulation (V/V_max)

which gives the optical density of 1 related to the standard optical pathlength of 1 m. Here emissivity and absorptivity is overestimated. The radiation source term is 3 times larger than the one using the WSGG model, and the same applies to all heat fluxes across the boundaries.

The radiation outlet boundary has a large impact on the radiation properties inside the chamber: setting the ambient temperature behind the outlet equal to outlet temperature, radiation from the environment penetrates the outlet and the temperature on the walls increase. As appropriate radiation outlet boundary condition one may apply an estimated black body temperature T_{blade} of the channel walls behind the combustion chamber.

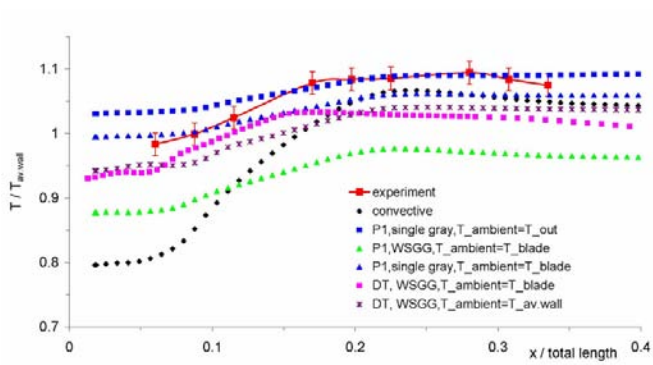

Figure 16: Temperature distribution at the ceramic interface, $T_{av.wall}$ refers to the area mean wall temperature as calculated (with WSGG DT

However, increasing the radiation black body outlet temperature from T_{blade} to $T_{av.wall}$ (with only a small radiation heat flux leaving the outlet), which is the average ceramic wall temperature based on the calculation with DT WSGG radiation modelling, does not change the temperature distribution along the ceramic wall very much. This is in particular true when the WSGG model is applied, with much lower emissivity values than the default single gray parameters in the standard application of the P1 radiation transport model in CFX. One can also see, that the application of the P1 radiation transport in combination with the WSGG model under predicts the wall temperature significantly. In this case, the radiative heat flux from the walls into the chamber exceeded the heat flux from the combustive medium to the walls, which is not realistic. Due to the discretization of the P1 model, a discontinuity can appear at the walls, which are not in thermodynamical equilibrium with the adjacent flow [14].

The WSGG model for rather optical thin media can be applied with the discrete transfer radiation transport, which predicts the shape of the measured temperature distribution very good. However it still under predicts the temperature values. The discrepancy is in a range of approximately 4% error. Possible reasons for this rather small discrepancy could be the imperfect temperature and species concentration fields of the numerical simulation. Furthermore, the discrepancy can stem from errors remaining in the radiation models employed such as the disregard of turbulence radiation interaction TRI.

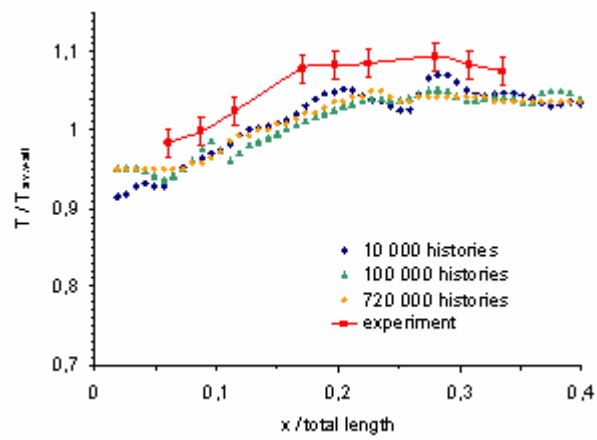

Figure 17: Temperature distribution at the ceramic interface, using Monte Carlo radiation transport

Since the experiment displayed turbulent conditions the turbulence-radiation interaction (TRI) may arise from the highly non-linear dependence of radiative transfer with respect to temperature and species concentrations [11]. Due to TRI radiative emission from a flame may be considerably higher than would be expected based on mean values of temperature and concentrations. The closure of TRI is a current field of research.

Any impact of the temperature function of the thermal conductivity of ceramics has been investigated separately. The

Copyright © 2007 by ASME

Downloaded From: https://proceedings.asmedigitalcollection.asme.org on 07/01/2019 Terms of Use: http://www.asme.org/about-asme/terms-of-use

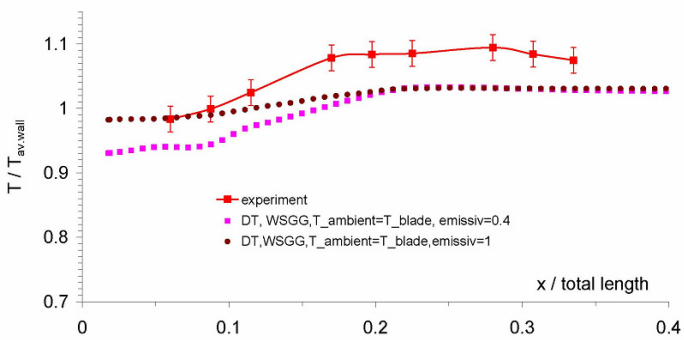

Figure 18: Impact of ceramic emissivity on the temperature distribution at the interface

application of the temperature function lowers the temperature distributions with an offset of around 20K, which increases the discrepancy to the experimental values even more.

The Monte Carlo approach leads to a wall temperature distribution similar to the result of the discrete transfer model. The number of histories has to be sufficiently high in order to reach a smooth temperature distribution, otherwise the slope becomes humpy due to a false discontinuous radiation distribution (fig.17).

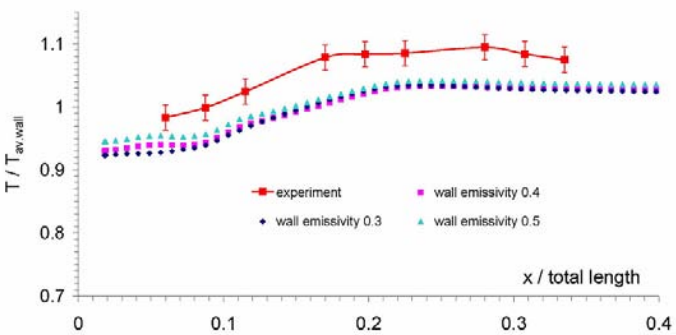

Figure 19: Impact of ceramic emissivity on the temperature distribution at the interface

Any alteration of the emissivity value at the ceramic interface changes the temperature distribution on the ceramic interface. Fig. 18 shows the result of a simulation, where the emissivity value of the ceramic tiles has been changed from 0.4 to 1 (from reflecting to black); the emissivity of the other liner walls has been kept constant 0.4. The temperature rises in the front part of the ceramic interface, upstream of the flow impingement on the wall. In this front area the radiation has the main contribution to the overall heat transfer, at the rear part convection dominates.

In the same way, any alteration of the wall emissivity has an impact on the temperature profile at the ceramic wall only at the front part, where radiation dominates. Fig. 19 shows the DT WSGG case of fig. 18 for various values of wall emissivity at all walls (0.5, 0.4 and 0.3). The small temperature drop takes place only at the front part of the wall, at the rear part convection dominates.

An uncertainty of the temperature at the liner cold side wall of about 4% (related to the preheat temperature) has also only a rather minor impact on the temperature distribution at the ceramic interface. Fig. 20 shows the result of the DT-WSGG simulation, where the liner cold side temperature distribution T-profile 1 is shown in fig.5. T-profile 2 is identical but has an offset of plus 4 % related to the preheat temperature. The temperatures at the liner hot side rise less than 1.5 % related to $T_{av.wall}$ (fig.20).

The radiative source term using the WSGG model is around 3% of the thermal power (450 kW). The radiative wall heat load makes up 20-30% of the convective wall heat load.

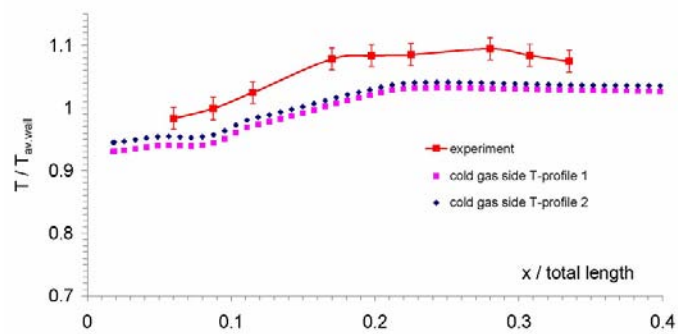

Figure 20: Impact of liner cold side temperature distribution on the temperature distribution at the ceramic hot gas side

CONCLUSIONS

In the present investigations it became clear, that in the case considered here radiation can be calculated in the postprocessing of a converged simulation of flow and combustion processes. Thus, it was found that the impact of the altered temperature field on the momentum transport can be neglected. For optical thin conditions, the P1 model as implemented in CFX is not recommended. It is possible to use the WSGG model separately to determine in a quick way the emissivities for the case under investigation. Here, the input parameters are operation pressure, species concentrations and temperature. The optical pathlength depends on the geometrical size of the application. Hence, it is possible to assess previous to the radiation modeling the optical density, which than, for example, can be used to assess the applicability of the efficient P1 radiation transport model.

Copyright © 2007 by ASME

Downloaded From: https://proceedings.asmedigitalcollection.asme.org on 07/01/2019 Terms of Use: http://www.asme.org/about-asme/terms-of-use

Further, dependent on the characteristics of the boundary layer at the wall, transient effects of the combustion flow might cause a significant alteration of the heat transfer [15]. A detailed numerical study on alteration in heat transfer due to transient boundary layer characteristics in unsteady flow is currently carried out at DLR [16].

Still, with steady state modeling of the combustion and treating the radiation as a post process, it was possible to reach fairly good agreement between experiment and simulation. The investigation shows, that radiation can have a significant contribution to wall heat load of gas turbine combustors even at atmospheric test conditions. In particular, radiation has a significant effect on the wall temperature distribution compared to the pure convective solution, and is not only an offset to the pure convective solution. Radiation can be taken into account with reasonable effort. For low optical density, the radiation transport models discrete transfer and Monte-Carlo performed well.

ACKNOWLEDGEMENTS

This work was funded by Siemens AG Power Generation, Mülheim a. d. Ruhr, Germany.

REFERENCES

[1] Stuttaford, P.J., P. A. Rubini, Assessment of a radiative heat transfer model for gas turbine combustor preliminary design, J. of Propulsion and Power, vol. 14, No. 1, 1998, 66-73

[2] Eklund, D.R., T. Badinand, T. Fransson, A numerical study of radiation effects in gas turbine combustion chambers, AIAA98-3822, 1998

[3] Andreini, A., A. Bacci, C. Carcasci, B. Facchini, A. Asti, G. Ceccherini, E. Del Puglia, R. Modi, Numerical heat transfer analysis of an innovative gas turbine combustor: coupled study of radiation and cooling in the upper part of the liner, ASME GT2005-68365

[4] Schildmacher K.-U., Koch R., Wittig S., Krebs W., Hoffmann S.; Experimental Investigations of Unsteady Flow Phenomena in High Intense Combustion Systems; proceedings of the 6th. European Conference on Industrial Furnaces and Boilers, 2002

[5] Schildmacher K.-U., Koch R.; Experimental Investigation of the Interaction of unsteady Flow with Combustion; Journal for Engineering for Gas Turbines and Power, Vol. 127 (2), pp. 295-300, 2005

[6] Kopitzki K.; Einführung in die Festkörperphysik; B. G. Teubner Studienbücher, Stuttgart 1989

[7] Wieser, W., T. Esch, F. Menter, Heat Transfer Predictions using Advanced Two-Equation Turbulence Models; CFX validation report CFX-VAL10/0602, Ansys CFX, 11.06.2002

[8] Hadvig S.; Gas emissivity and absorptivity: A thermodynamic study; Journal of the Institute of Fuel, April 1970, pp. 129-135

[9] Edwards D.K. and Matavosian R.; Scaling rules for total absorptivity and emissivity of gases; Transactions of the ASME, Journal of Heat Transfer, November 1984, Vol. 106, pp. 684-689.

[10] Taylor P.B. and Foster P.J.; The total emissivities of luminous and non-luminous flames; Int. Journal Heat Mass Transfer, Vol. 17, 1974, pp. 1591-1605

[11] Modest M. F.; Radiative Heat Transfer; Academic Press (Elsevier Science), USA 2003

[12] Manual CFX5, Solver Modeling – Radiation Modeling

[13] Siegel R., Howell J.R. and Lohrengel J.; Wärmeübertragung durch Strahlung; Reihe Wärme- und Stoffübertragung, ed. U. Grigull, Springer Verlag 1988

[14] Krebs, W.; Mehrdimensionaler Strahlungswärmeübergang an Gasturbinen-Brennkammerwände: Entwicklung und Überprüfung von Berechnungsverfahren; Dissertation, Fakultät für Maschinenbau, Universität Karlsruhe (TH)

[15] Ishino Y., Suzuki M., Abe T., Ohiwa N. and Yamaguchi S.; Flow and heat Transfer Characteristics in Pulsating Pipe Flows (Effects of Pulsation on Internal Heat Transfer in a Circular Pipe Flow); heat transfer-Japanese Research,25 (5), 1996, pp. 323-341.

[16] Panara D., Porta M., Dannecker R. and Noll B.; Wall-Functions and Boundary Layer Response to Pulsating and Oscillating Turbulent Channel Flows; 5th International Symposium on Turbulence, Heat and Mass Transfer THMT06; Dubrovnik, Croatia, September 25-29, 2006

Copyright © 2007 by ASME

Downloaded From: https://proceedings.asmedigitalcollection.asme.org on 07/01/2019 Terms of Use: http://www.asme.org/about-asme/terms-of-use